INTERNATIONAL JOURNAL FOR NUMERICAL METHODS IN FLUIDS
Int. J. Numer. Meth. Fluids 2003; **41**:841–861 (DOI: 10.1002/fld.471)

Central schemes for open-channel flow

Guido Gottardi[1,*,†] and Maurizio Venutelli[2,‡]

[1] *Dipartimento di Ingegneria Chimica, Mineraria e delle Tecnologie Ambientali, Università di Bologna, I-40136 Bologna, Italy*
[2] *Dipartimento di Ingegneria Civile, Università di Pisa, I-56126 Pisa, Italy*

SUMMARY

The resolution of the Saint-Venant equations for modelling shock phenomena in open-channel flow by using the second-order central schemes of Nessyahu and Tadmor (NT) and Kurganov and Tadmor (KT) is presented. The performances of the two schemes that we have extended to the non-homogeneous case and that of the classical first-order Lax–Friedrichs (LF) scheme in predicting dam-break and hydraulic jumps in rectangular open channels are investigated on the basis of different numerical and physical conditions. The efficiency and robustness of the schemes are tested by comparing model results with analytical or experimental solutions. Copyright © 2003 John Wiley & Sons, Ltd.

KEY WORDS: Saint-Venant equations; open-channel flow; shock phenomena; central difference schemes; dam-break; hydraulic jump

1. INTRODUCTION

Correctly representing and simulating shock phenomena involves considerable difficulties but is of primary interest in hydraulic engineering as well as in other applied mathematical analysis.

Assuming the shock phenomena in open-channel flow to be appropriately described by the non-linear set of hyperbolic Saint-Venant equations, past scientific contributions in this field have been concerned with the schemes for the numerical integration of these equations, and in particular with the so called *shock-capturing schemes* [1].

Many of these schemes use the Godunov approach [2], for which each time-step consists of three stages: *reconstruction*, *evolution* and *projection*. With regard to the evolution stage, we distinguish in the scientific literature between upwind and central Godunov-type schemes.

*Correspondence to: G. Gottardi, Dipartimento di Ingegneria Chimica, Mineraria e delle Tecnologie Ambientali, Università di Bologna, I-40136 Bologna, Italy.
†E-mail: guido.gottardi.1@mail.ing.unibo.it
‡E-mail: m.venutelli@ing.unipi.it

Received 17 April 2002
Revised 30 October 2002

Upwind schemes sample the reconstructed values at the mid-cells, whereas, central schemes are based on staggered sampling at the interfacing break-points. Central schemes present the principal advantage of simplicity in that no approximate Riemann solvers are involved in their construction.

The first-order Lax–Friedrichs (LF) scheme [3, 4] is the forerunner of all the central schemes, but its great numerical dissipation limits its use for modelling shock conditions. A second-order extension of the LF scheme is presented in the Nessyahu–Tadmor (NT) scheme [5]. In this model, the first-order piecewise constant solution of the LF scheme is replaced by a MUSCL-type second-order piecewise linear approximation. As the complete Saint-Venant equations contain a source term, we present a formulation of the NT scheme for the non-homogeneous case. Recently, a new second-order Kurganov–Tadmor (KT) central scheme has been introduced for solving homogeneous convection and convection–diffusion equations [6]. In this scheme the evolution stage is performed by integrating over non-uniform control volumes (cells), whose sizes are proportional to the local speeds of the propagation of the wave. The evolved solution, after an additional reconstruction, is then projected back onto the original grid.

In this paper, we have extended this central scheme also to the non-homogeneous case. The integration in time of this scheme has been obtained by using a third-order TVD Runge–Kutta method. The simplicity of application and the accuracy of the solutions of the NT and KT central schemes in simulating shocks in open channel flows, by using Saint-Venant equations, are presented. These test cases present the results of simulations regarding dam-break and hydraulic jump phenomena.

The paper is organized as follows. In Section 2 we recall the set of Saint-Venant equations governing unsteady open-channel flow. In Section 3 we recall the philosophy of Godunov-type central schemes, the first-order LF scheme, the second-order NT schemes, and the first- and second-order fully discrete and semi-discrete KT schemes. In Section 4 we present a series of numerical simulations of dam-break and hydraulic jump tests cases, implemented by the schemes of Section 3. Conclusions of this work are drawn in Section 5.

2. GOVERNING EQUATIONS

The mathematical basis of one-dimensional unsteady open-channel flow is governed by Saint–Venant equations. The set of partial differential, continuity and momentum equations, can be written in the following form [7],

$$\frac{\partial A}{\partial t} + \frac{\partial Q}{\partial x} = 0 \tag{1a}$$

$$\frac{\partial Q}{\partial t} + \frac{\partial}{\partial x}\left(\frac{Q^2}{A} + gI_1\right) = gI_2 + gA(S_0 - S_f) \tag{1b}$$

here, $A = A(x,t)$ is the wetted cross-sectional area, $Q = Q(x,t)$ the discharge, x is the spatial co-ordinate, assumed positive along the flow direction, t is the time, g the acceleration due to gravity, S_0 is the bed slope, and S_f the friction slope. Applying, for its evaluation, the

Manning's formula, we have

$$S_{\mathrm{f}} = \frac{n_m^2 Q|Q|}{A^2 R^{4/3}}$$

in which n_m ($\mathrm{m}^{-1/3}\mathrm{s}$) is the roughness coefficient and R the hydraulic radius.

In Equation (1b), the term I_1 represents the hydrostatic pressure force term, while I_2 represents the pressure force due to longitudinal width variations which are expressed as

$$I_1 = \int_0^{h(x,t)} (h-\eta) b(x,\eta)\,\mathrm{d}\eta, \quad I_2 = \int_0^{h(x,t)} (h-\eta)\frac{\partial b(x,\eta)}{\partial x}\,\mathrm{d}\eta$$

where h is the water depth, η is the depth integration variable along the vertical axis, b is the width of the cross section such that $b(x,h) = B(x) =$ free surface width. In rectangular channels with width B, we obtain $I_1 = \frac{1}{2}A^2/B$ and $I_2 = 0$. It is possible to write the set of Equations (1) in the following compact vectorial form

$$w_t + f_x(w) = z(w) \tag{2}$$

here, $w_t := \partial w/\partial t$, $f_x := \partial f/\partial x$, and w, f, and z are, respectively, the conserved variable, the flux function, and the forcing term, expressed in this case by the following two component vectors:

$$w = \begin{bmatrix} A \\ Q \end{bmatrix}, \quad f = \begin{bmatrix} Q \\ \dfrac{Q^2}{A} + g\dfrac{A^2}{2B} \end{bmatrix}, \quad z = \begin{bmatrix} 0 \\ gA(S_0 - S_{\mathrm{f}}) \end{bmatrix} \tag{3}$$

The Jacobian matrix $J = \partial f/\partial w$ of this system is

$$J = \begin{bmatrix} 0 & 1 \\ g\dfrac{A}{B} - \dfrac{Q^2}{A^2} & 2\dfrac{Q}{A} \end{bmatrix} = \begin{bmatrix} 0 & 1 \\ c^2 - u^2 & 2u \end{bmatrix} \tag{4}$$

where $u = Q/A$ is the mean velocity and $c = (gA/B)^{1/2}$ is the celerity. The eigenvalues of J are

$$\lambda_{1,2} = u \pm c \tag{5a,b}$$

For width $B = 1$, the vectors (3), may be written in the form

$$w = \begin{bmatrix} h \\ hu \end{bmatrix}, \quad f = \begin{bmatrix} hu \\ hu^2 + \frac{1}{2}gh^2 \end{bmatrix}, \quad z = \begin{bmatrix} 0 \\ gh(S_0 - S_{\mathrm{f}}) \end{bmatrix} \tag{6}$$

The set of Equations (2) are completed by the initial conditions $w(x, t=0) = w_0(x)$ and by appropriate boundary conditions.

3. CENTRAL SCHEMES

The double integration in space and time over the rectangle $I_x \times [t, t+\Delta t]$ of the set of hyperbolic Equations (2), with $I_x := [x - \Delta x/2, x + \Delta x/2]$, Δx and Δt being the space and

time steps, respectively, gives

$$\bar{w}(x,t+\Delta t)=\bar{w}(x,t)-\frac{1}{\Delta x}\left[\int_t^{t+\Delta t} f\left(w\left(x+\frac{\Delta x}{2},t\right)\right)\mathrm{d}t-\int_t^{t+\Delta t} f\left(w\left(x-\frac{\Delta x}{2},t\right)\right)\mathrm{d}t\right]$$
$$+\frac{1}{\Delta x}\int_t^{t+\Delta t}\int_{x-\frac{\Delta x}{2}}^{x+\frac{\Delta x}{2}} z(w(x,t))\mathrm{d}x\,\mathrm{d}t \tag{7}$$

where

$$\bar{w}(x,t):=\frac{1}{\Delta x}\int_{x-\frac{\Delta x}{2}}^{x+\frac{\Delta x}{2}} w(x,t)\mathrm{d}x$$

indicates the sliding average of $w(\cdot,t)$. Equation (7) is the starting point of Godunov-type general schemes for the integration of the set of Equations (2).

Now, if we construct a piecewise approximation $v(\cdot,t)$ of $w(\cdot,t)$, at the discrete time level $t^n=n\Delta t$, in the form

$$w(x,t^n)\simeq v(x,t^n)=\sum_j p_j^n(x)1_{I_j} \tag{8}$$

Here, $\{p_j^n\}$ are algebraic polynomials supported in the discrete cells $I_j:=[x_{j-1/2},x_{j+1/2}]$ with cell boundaries in the points $x_{j-1/2}:=(j-\frac{1}{2})\Delta x$ and $x_{j+1/2}:=(j+\frac{1}{2})\Delta x$, and 1_{I_j} is a function which equals one inside the discrete cell I_j and zero outside I_j. The $\{p_j^n\}$ polynomials are centred around the midpoints $x_j=j\Delta x$ so, in the cell interval I_j, we have $\tilde{p}_j(x)=w(x_j,t^n)$.

The time evolution of the piecewise approximation $v(x,t^n)$, on the basis of (7), reads

$$\bar{v}(x,t^{n+1})=\bar{v}(x,t^n)-\frac{1}{\Delta x}\left[\int_{t^n}^{t^{n+1}} f\left(v\left(x+\frac{\Delta x}{2},t\right)\right)\mathrm{d}t-\int_{t^n}^{t^{n+1}} f\left(v\left(x-\frac{\Delta x}{2},t\right)\right)\mathrm{d}t\right]$$
$$+\frac{1}{\Delta x}\int_{t^n}^{t^{n+1}}\int_{x-\frac{\Delta x}{2}}^{x+\frac{\Delta x}{2}} z(v(x,t))\,\mathrm{d}x\,\mathrm{d}t \tag{9}$$

To construct a Godunov-type scheme, we apply (9) at discrete grid points. Here we distinguish between two main methods, corresponding, respectively, to the upwind and central schemes, according to the way of sampling Equation (9). The upwind schemes are obtained by sampling (9) at the mid-cells, $x=x_j$. This method uses non-staggered grids-cells $[x_{j-1/2},x_{j+1/2}]$ for the evolution step, and must, therefore, rely on the solution of exact or approximate Riemann problem solvers at the grid-cell interfaces, for calculating numerical fluxes. Instead, the Godunov-type central schemes are based on sampling Equation (9) on the interfacing breakpoints $x=x_{j+1/2}$ [8]. For these schemes the space integration is performed on staggered grid-cells $[x_j,x_{j+1}]$. The evolution scheme obtained in this case is

$$\bar{v}_{j+1/2}^{n+1}=\bar{v}_{j+1/2}^n-\frac{1}{\Delta x}\left[\int_{t^n}^{t^{n+1}} f(v(x_{j+1},t))\,\mathrm{d}t-\int_{t^n}^{t^{n+1}} f(v(x_j,t))\,\mathrm{d}t\right]+G_{j+1/2}^n \tag{10}$$

in which the staggered averages $\bar{v}^n_{j+1/2}$ are given by

$$\bar{v}^n_{j+1/2} = \frac{1}{\Delta x}\left[\int_{x_j}^{x_{j+1/2}} p^n_j(x)\,\mathrm{d}x + \int_{x_{j+1/2}}^{x_{j+1}} p^n_{j+1}(x)\,\mathrm{d}x\right] \tag{11}$$

and the source terms are

$$G^n_{j+1/2} = \frac{1}{\Delta x}\int_{t^n}^{t^{n+1}}\left[\int_{x_j}^{x_{j+1/2}} z(v(x,t))\,\mathrm{d}x + \int_{x_{j+1/2}}^{x_{j+1}} z(v(x,t))\,\mathrm{d}x\right]\mathrm{d}t \tag{12}$$

For these staggered methods, differently from the non-staggered methods, the numerical fluxes are evaluated in smooth regions where no jump discontinuities occur, so Riemann problem are no longer to be solved. Staggered methods, however, tend to smear out contact discontinuities when small time steps are used. This implies that slowly moving waves will present a large amount of diffusion. Different schemes are obtained by changing the polynomial representation $p_j(x)$ of the variables within each grid-cell, i.e. piecewise-constant, piecewise-linear, piecewise-quadratic, which originate, respectively, first-order, second-order, and third-order central schemes.

3.1. First-order Lax–Friedrichs (LF) scheme

The first-order LF central scheme [3, 4], is obtained from (10) to (12), by using for the reconstruction step a piecewise constant polynomial form $p^n_j(x) = \bar{v}^n_j = w^n_j$ of the variables within the cell $[x_{j-1/2}, x_{j+1/2}]$, and by considering constant (i.e. evaluated at time $t = n\Delta t$) the fluxes and the forcing terms in the integrals of (10) and (12), respectively. In this way we obtain

$$\bar{w}^{n+1}_{j+1/2} = \frac{1}{2}(\bar{w}^n_j + \bar{w}^n_{j+1}) - \sigma[f(w^n_{j+1}) - f(w^n_j)] + \frac{\Delta t}{2}[z(w^n_j) + z(w^n_{j+1})] \tag{13}$$

where $\sigma = \Delta t/\Delta x$ is the fixed mesh ratio, and $w^n_j := w(x_j, t^n) = \bar{w}^n_j$.

The non-staggered cell-average at time t^{n+1}, $\bar{w}^{n+1}_j$, obtained as the average of two neighbouring staggered cell-averages reads [11]

$$\begin{aligned}\bar{w}^{n+1}_j := \frac{1}{2}(\bar{w}^{n+1}_{j-1/2} + \bar{w}^{n+1}_{j+1/2}) &= \frac{1}{4}(\bar{w}^n_{j-1} + 2\bar{w}^n_j + \bar{w}^n_{j+1}) \\ &- \frac{\sigma}{2}[f(w^n_{j+1}) - f(w^n_{j-1})] + \frac{\Delta t}{4}[z(w^n_{j-1}) + 2z(w^n_j) + z(w^n_{j+1})]\end{aligned} \tag{14}$$

Equations (13) and (14) constitute the two-step explicit procedure of the LF central scheme. The schematic representation of this scheme is given in Figure 1.

3.2. Second-order Nessyahu–Tadmor (NT) scheme

A natural extension of the LF scheme is the second-order NT scheme [5], also defined by Erbes [9], high-resolution Lax–Friedrichs scheme. For this method, the piecewise-linear

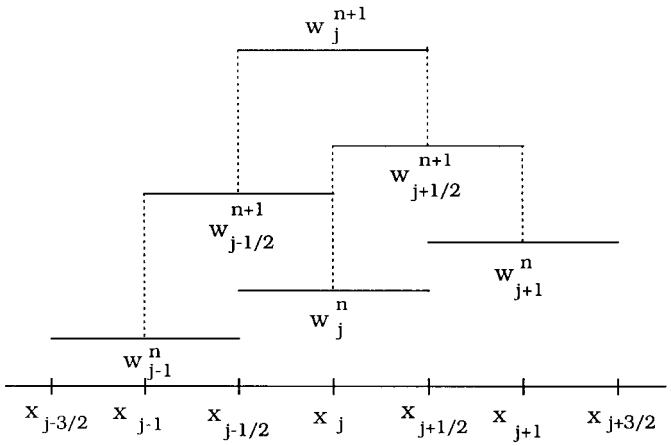

Figure 1. Lax–Friedrichs scheme.

MUSCL-type approximation [10] on the cell $I_j := [x_{j-1/2}, x_{j+1/2}]$ is used

$$p_j^n(x) = w_j^n + (x - x_j)(w_x)_j^n, \quad x_{j-1/2} \leqslant x \leqslant x_{j+1/2} \tag{15a}$$

$$w(x, t^n) \simeq \sum_j p_j(x) 1_{I_j} \tag{15b}$$

here, $\bar{p}_j^n(x) = \bar{w}_j^n = w_j^n$ is the computed cell average and $(w_x)_j^n$ indicates an approximation of the exact derivative $w_x(x_j, t^n)$. A possible computation of $(w_x)_j^n$ is given by the family of discrete derivatives parameterized with $1 \leqslant \theta \leqslant 2$; i.e. for any grid function $\{w_j\}$ we set [11]

$$(w_x)_j^n = \mathrm{MM}\{\theta(w_{j+1}^n - w_j^n)/\Delta x, (w_{j+1}^n - w_{j-1}^n)/2\Delta x, \theta(w_j^n - w_{j-1}^n)/\Delta x\} \tag{16}$$

here, MM denotes the MinMod non-linear limiter function, defined as

$$\mathrm{MM}\{x_1, x_2, \ldots\} = \begin{cases} \min_j\{x_j\} & \text{if } x_j > 0, \ \forall j \\ \max_j\{x_j\} & \text{if } x_j < 0, \ \forall j \\ 0 & \text{otherwise} \end{cases} \tag{17}$$

The evolution in time of the interpolant (15) over the staggered cells to the next time step, t^{n+1}, obtained by (10)–(12), gives the following two-step *predictor–corrector* form of the NT scheme

$$w_j^{n+1/2} = w_j^n - \frac{\Delta t}{2}\left[\frac{f(w_{j+1}^n) - f(w_j^n)}{\Delta x} - z(w_j^n)\right] \tag{18a}$$

$$\bar{w}_{j+1/2}^{n+1} = \frac{1}{2}(\bar{w}_j^n + \bar{w}_{j+1}^n) + \frac{\Delta x}{8}[(w_x)_j^n - (w_x)_{j+1}^n] - \sigma[f(w_{j+1}^{n+1/2}) - f(w_j^{n+1/2})]$$
$$+ \frac{\Delta t}{4}[z(w_j^{n+1/2}) + z(w_{j+1/2}^{-n+1/2}) + z(w_{j+1/2}^{+n+1/2}) + z(w_{j+1}^{n+1/2})] \tag{18b}$$

here, the values of $w_j^{n+1/2}$ and $w_{j+1}^{n+1/2}$ are computed by (18a) by using Taylor's series [5], and Equation (2), moreover, the derivatives $(w_x)_j^n$, $(w_x)_{j+1}^n$ are evaluated by (16). The flux and source terms are considered constant in time and evaluated at time $t^{n+1/2}$, moreover, we have assumed the source term, $z(w(x,t))$, to have a linear behaviour in terms of x inside the intervals $[x_j, x_{j+1/2}]$ and $[x_{j+1/2}, x_{j+1}]$. The left and right values of w at point $x_{j+1/2}$ are

$$w_{j+1/2}^{-n+1/2} = w_j^{n+1/2} + \frac{\Delta x}{2}(w_x)_j^{n+1/2} \tag{19a}$$

$$w_{j+1/2}^{+n+1/2} = w_{j+1}^{n+1/2} - \frac{\Delta x}{2}(w_x)_{j+1}^{n+1/2} \tag{19b}$$

where $(w_x)_j^{n+1/2}$ and $(w_x)_{j+1}^{n+1/2}$ are evaluated by (16). A different formulation of the source term, based on the integration in the interval $[x_j, x_{j+1}]$ inside which a linear behaviour assumed in terms of x for z, has been presented in Reference [12].

In order to transform the staggered second-order scheme (18b) into a non-staggered scheme, as a first step, we reconstruct a piecewise-linear interpolant through the calculated staggered cell-averages at time t^{n+1},

$$w_{j\pm1/2}^{n+1} = \bar{w}_{j\pm1/2}^{n+1} + (w_x)_{j\pm1/2}^{n+1}(x - x_{j\pm1/2}) \tag{20}$$

as a second step, the cell-averages at the next time step, $\bar{w}_j^{n+1}$, are obtained by averaging this interpolant, resulting in the following non-staggered corrector scheme [11]

$$\begin{aligned}
\bar{w}_j^{n+1} &= \frac{1}{\Delta x}\left[\int_{x_{j-1/2}}^{x_j} w_{j-1/2}^{n+1}\,\mathrm{d}x + \int_{x_j}^{x_{j+1/2}} w_{j+1/2}^{n+1}\,\mathrm{d}x\right] \\
&= \frac{1}{4}(\bar{w}_{j-1}^n + 2\bar{w}_j^n + \bar{w}_{j+1}^n) - \frac{\Delta x}{16}\left[(w_x)_{j+1}^n - (w_x)_{j-1}^n\right] \\
&\quad - \frac{\sigma}{2}\left[f(w_{j+1}^{n+1/2}) - f(w_{j-1}^{n+1/2})\right] - \frac{\Delta x}{8}\left[(w_x)_{j+1/2}^{n+1} - (w_x)_{j-1/2}^{n+1}\right] \\
&\quad + \frac{\Delta t}{8}\left[z(w_{j-1}^{n+1/2}) + 2z(w_j^{n+1/2}) + z(w_{j+1}^{n+1/2})\right. \\
&\quad \left. + z(w_{j-1/2}^{-n+1/2}) + z(w_{j-1/2}^{+n+1/2}) + z(w_{j+1/2}^{-n+1/2}) + z(w_{j+1/2}^{+n+1/2})\right]
\end{aligned} \tag{21a}$$

where

$$(w_x)_{j-1/2}^{n+1} = \frac{1}{\Delta x}\,\mathrm{MM}(\bar{w}_{j+1/2}^{n+1} - \bar{w}_{j-1/2}^{n+1}, \bar{w}_{j-1/2}^{n+1} - \bar{w}_{j-3/2}^{n+1}) \tag{21b}$$

Here, MM is the MinMod non-linear limiter defined in (17), and $(w_x)_{j+1/2}^{n+1}$ is obtained by replacing $j+1$ in place of j in all the RHS terms of (21b). Equations (18a), (18b) and (19) constitute the three-step explicit procedure of the NT central scheme. A schematic representation of this scheme is given in Figure 2.

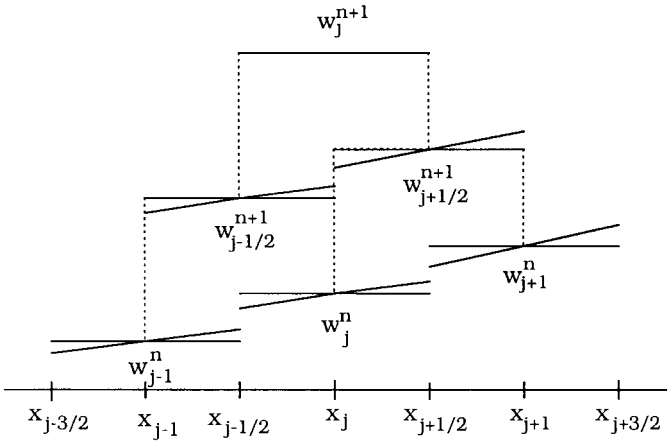

Figure 2. Nessyahu–Tadmor scheme.

3.3. *First- and second-order Kurganov–Tadmor (KT) schemes*

In the NT schemes, the length of the spatial cells Δx remains constant in time, whereas, in the new central schemes KT, proposed by Kurganov and Tadmor [6], for solving the homogeneous case of (2), the space steps are not constant in time, and their lengths are computed following the local values of the propagation wave celerities. For each time step $\Delta t = t^{n+1} - t^n$, the reconstruction is obtained by using the piecewise-linear polynomial of Equations (15) for the cells $\Delta x_{j+1/2}$ and Δx_j defined by

$$\Delta x_{j+1/2} := x^n_{j+1/2,r} - x^n_{j+1/2,l}, \quad \Delta x_j := x^n_{j+1/2,l} - x^n_{j-1/2,r} \tag{22a}$$

where

$$x^n_{j\pm1/2,l} := x^n_{j\pm1/2} - a^n_{j\pm1/2}\Delta t, \quad x^n_{j\pm1/2,r} := x^n_{j\pm1/2} + a^n_{j\pm1/2}\Delta t \tag{22b}$$

Here, $a_{j+1/2}$ is the maximum value of the propagation celerity of the point $x_{j+1/2}$, defined by

$$a_{j+1/2} := \max\{\rho(J(w^+_{j+1/2})), \rho(J(w^-_{j+1/2}))\} \tag{23}$$

where $\rho(J) := \max_i |\lambda_i|$, in which λ_i are the eigenvalues of the Jacobian matrix J given by (5), and the right and left values of w at point $x_{j+1/2}$ are, respectively,

$$w^+_{j+1/2} := p^n_{j+1}(x_{j+1/2}) = w^n_{j+1} - \frac{1}{2}(w_x)^n_{j+1}\Delta x \tag{24a}$$

$$w^-_{j+1/2} := p^n_j(x_{j+1/2}) = w^n_j + \frac{1}{2}(w_x)^n_j\Delta x \tag{24b}$$

Here, the approximate derivative $(w_x)^n_j$ is given by

$$(w_x)^n_j = \frac{1}{\Delta x}\,\mathrm{MM}(w^n_j - w^n_{j-1},\, w^n_{j+1} - w^n_j) \tag{25}$$

For each time step, we start from the following piecewise linear polynomial approximation at time level $t = t^n := n\Delta t$

$$w(x,t^n) = \sum_j p_j^n(x) 1_{I_j}, \quad p_j^n(x) := w_j^n + (x - x_j)(w_x)_j^n, \quad I_j := [x_{j-1/2}, x_{j+1/2}] \tag{26}$$

where $\bar{p}_j^n(x) = w_j^n = \bar{w}_j^n$. By using (10), where for the homogeneous case the source term $G_{j+1/2} = 0$, we proceed with the exact evaluation of cell averages $\omega_{j+1/2}^{n+1}$, ω_j^{n+1} at t^{n+1}, based on the integration over the space intervals $[x_{j+1/2,l}, x_{j+1/2,r}]$, and $[x_{j-1/2,r}, x_{j+1/2,l}]$, respectively. Moreover, by using the midpoint rule to approximate the flux integrals on RHS of (10), we obtain [6]

$$\begin{aligned}
\omega_{j+1/2}^{n+1} &:= \frac{1}{\Delta x_{j+1/2}} \int_{x_{j+1/2,l}}^{x_{j+1/2,r}} w(x,t^{n+1})\,\mathrm{d}x \\
&= \frac{w_j^n + w_{j+1}^n}{2} + \frac{\Delta x - a_{j+1/2}^n \Delta t}{4}\left((w_x)_j^n - (w_x)_{j+1}^n\right) \\
&\quad - \frac{1}{2a_{j+1/2}^n}[f(w_{j+1/2,r}^{n+1/2}) - f(w_{j+1/2,l}^{n+1/2})] \qquad (27a) \\
\omega_j^{n+1} &:= \frac{1}{\Delta x_j} \int_{x_{j-1/2,r}}^{x_{j+1/2,l}} w(x,t^{n+1})\,\mathrm{d}x \\
&= w_j^n + \frac{\Delta t}{2}(a_{j-1/2}^n - a_{j+1/2}^n)(w_x)_j^n \\
&\quad - \frac{\sigma}{1 - \sigma(a_{j-1/2}^n + a_{j+1/2}^n)}[f(w_{j+1/2,l}^{n+1/2}) - f(w_{j+1/2,r}^{n+1/2})] \qquad (27b)
\end{aligned}$$

Here, the midpoint values are obtained by the corresponding Taylor expansion

$$w_{j+1/2,l}^{n+1/2} := w_{j+1/2,l}^n - \frac{\Delta t}{2} f_x(w_{j+1/2,l}^n), \quad w_{j+1/2,l}^n := w_j^n + \Delta x (w_x)_j^n \left(\frac{1}{2} - \sigma a_{j+1/2}^n\right) \tag{28a}$$

$$w_{j+1/2,r}^{n+1/2} := w_{j+1/2,r}^n - \frac{\Delta t}{2} f_x(w_{j+1/2,r}^n), \quad w_{j+1/2,r}^n := w_{j+1}^n - \Delta x (w_x)_{j+1}^n \left(\frac{1}{2} - \sigma a_{j+1/2}^n\right) \tag{28b}$$

Now to obtain the averages over the original, non-staggered cells $[x_{j-1/2}, x_{j+1/2}]$, we use the following piecewise linear reconstruction over the non-uniform cells at $t = t^{n+1}$, and we project its averages back onto the original uniform grid

$$\tilde{\omega}(x,t^{n+1}) := \sum_j \{[\omega_{j+1/2}^{n+1} + (w_x)_{j+1/2}^{n+1}(x - x_{j+1/2})] 1_{[x_{j+1/2,l}^n, x_{j+1/2,r}^n]} + \omega_j^{n+1} 1_{[x_{j-1/2,r}^n, x_{j+1/2,l}]}\} \tag{29}$$

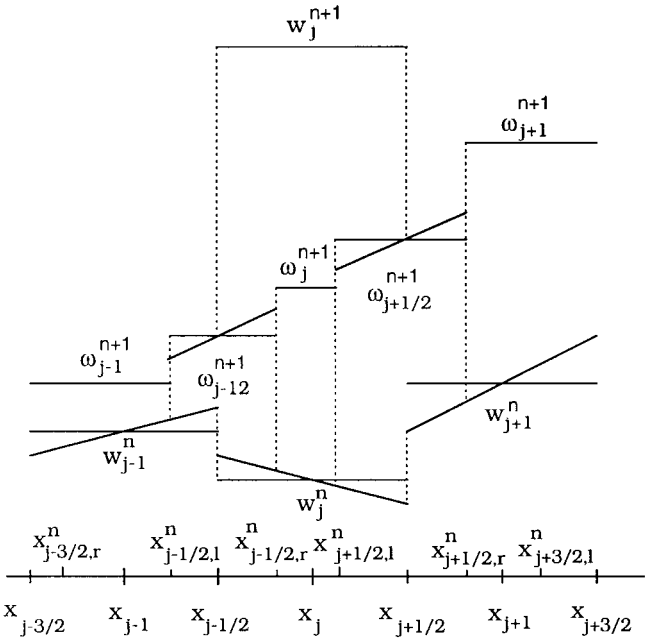

Figure 3. Kurganov–Tadmor scheme.

Here, the spatial derivative $w_x(x_{j+1/2}, t^{n+1})$ is approximated by

$$(w_x)_{j+1/2}^{n+1} = \frac{2}{\Delta x}\,\mathrm{MM}\left(\frac{\omega_{j+1}^{n+1} - \omega_{j+1/2}^{n+1}}{1+\sigma(a_{j+1/2}^n - a_{j+3/2}^n)}, \frac{\omega_{j+1/2}^{n+1} - \omega_j^{n+1}}{1+\sigma(a_{j+1/2}^n - a_{j-1/2}^n)}\right) \tag{30}$$

Finally, the fully discrete second-order central KT scheme is obtained by averaging the approximate solution in (27) into the non-staggered cells $[x_{j-1/2}, x_{j+1/2}]$. In this way we obtain

$$\begin{aligned} w_j^{n+1} = \frac{1}{\Delta x}\int_{x_{j-1/2}}^{x_{j+1/2}} \tilde{\omega}(x, t^{n+1})\,\mathrm{d}x = \sigma a_{j-1/2}^n \omega_{j-1/2}^{n+1} + [1-\sigma(a_{j-1/2}^n + a_{j+1/2}^n)]\omega_j^{n+1} \\ + \sigma a_{j+1/2}^n \omega_{j+1/2}^{n+1} + \frac{\Delta x}{2}[(\sigma a_{j-1/2}^n)^2 (w_x)_{j-1/2}^{n+1} - (\sigma a_{j+1/2}^n)^2 (w_x)_{j+1/2}^{n+1}] \end{aligned} \tag{31}$$

where the intermediate value, $\omega_{j-1/2}^{n+1}$, the spatial derivative, $(w_x)_{j-1/2}^{n+1}$, the midvalues, $w_{j-1/2,l}^{n+1/2}$, $w_{j-1/2,r}^{n+1/2}$ are readily obtained from (27a), (30), (28a) and (28b), respectively, by replacing $j-1$ in place of j in all the space indices of their RHS terms. A schematic representation of the KT scheme is given in Figure 3.

The following first-order version of the KT scheme, originally attributed to Rusanov [6], is obtained from (31) by setting both the slopes, $(w_x)_j^n$ and $(w_x)_{j+1}^n$ to be zero, as can be seen

by inspecting (27) and (28),

$$w_j^{n+1} = w_j^n - \frac{\sigma}{2}[f(w_{j+1}^n) - f(w_{j-1}^n)] + \frac{1}{2}[\sigma a_{j+1/2}^n (w_{j+1}^n - w_j^n) - \sigma a_{j-1/2}^n (w_j^n - w_{j-1}^n)] \tag{32}$$

3.3.1. Semi-discrete formulation of KT schemes. If we substitute into the fully discrete second-order KT central scheme (31) the terms of the cell averages, $\omega_{j\pm1/2}^{n+1}$, ω_j^{n+1}, and if we note that as $\Delta t \to 0$ the midvalues on the right of Equations (28) approach to

$$\begin{aligned} w_{j+1/2,l}^{n+1/2} &\to w_j(t) + \frac{\Delta x}{2}(w_x)_j(t) =: w_{j+1/2}^-(t) \\ w_{j+1/2,r}^{n+1/2} &\to w_{j+1}(t) - \frac{\Delta x}{2}(w_x)_{j+1}(t) =: w_{j+1/2}^+(t) \end{aligned} \tag{33}$$

We obtain from (31), as $\Delta t \to 0$, the semi-discrete second-order KT central scheme [6, 13]

$$\begin{aligned} \frac{\mathrm{d}}{\mathrm{d}t} w_j(t) = &-\frac{1}{2\Delta x}[(f(w_{j+1/2}^+(t)) + f(w_{j+1/2}^-(t))) - (f(w_{j-1/2}^+(t)) + f(w_{j-1/2}^-(t)))] \\ &+ \frac{1}{2\Delta x}\{a_{j+1/2}(t)[w_{j+1/2}^+(t) - w_{j+1/2}^-(t)] - a_{j-1/2}(t)[w_{j-1/2}^+(t) - w_{j-1/2}^-(t)]\} \end{aligned} \tag{34}$$

which can also be written in the following conservative form

$$\frac{\mathrm{d}}{\mathrm{d}t} w_j(t) = -\frac{H_{j+1/2}(t) - H_{j-1/2}(t)}{\Delta x} \tag{35}$$

with the numerical fluxes given by

$$H_{j\pm1/2}(t) = \frac{f(w_{j\pm1/2}^+(t)) + f(w_{j\pm1/2}^-(t))}{2} - \frac{a_{j\pm1/2}(t)}{2}[w_{j\pm1/2}^+(t) - w_{j\pm1/2}^-(t)] \tag{36}$$

Here, the intermediate values $w_{j\pm1/2}^{\pm}$ are given by Taylor expansions

$$w_{j+1/2}^+(t) := w_{j+1}(t) - \frac{\Delta x}{2}(w_x)_{j+1}(t), \quad w_{j+1/2}^-(t) := w_j(t) + \frac{\Delta x}{2}(w_x)_j(t) \tag{37a}$$

$$w_{j-1/2}^+(t) := w_j(t) - \frac{\Delta x}{2}(w_x)_j(t), \quad w_{j-1/2}^-(t) := w_{j-1}(t) + \frac{\Delta x}{2}(w_x)_{j-1}(t) \tag{37b}$$

Now, starting from the full discrete first-order KT central scheme (34) and setting $\Delta t \to 0$, we obtain the corresponding semi-discrete first-order central KT scheme [6],

$$\begin{aligned} \frac{\mathrm{d}}{\mathrm{d}t} w_j(t) = &-\frac{f(w_{j+1}(t) - f(w_{j-1}(t))}{2\Delta x} \\ &+ \frac{1}{2\Delta x}[a_{j+1/2}(t)(w_{j+1}(t) - w_j(t)) - a_{j-1/2}(t)(w_j(t) - w_{j-1}(t))] \end{aligned} \tag{38}$$

Semi-discrete schemes are particularly important for solving multidimensional non-linear conservation law and convection–diffusion problems. Some difficulties due to the numerical dissipation arise in using small time steps, with NT or LF schemes. When a semi-discrete scheme is coupled with an effective ordinary differential equation (ODE) solver, it is possible to overcome the numerical viscosity proportional to the vanishing size of the time step Δt, but, unfortunately, NT and LF schemes do not admit a semi-discrete form.

3.3.2. Extension of the KT scheme to the non-homogeneous case. A possible extension to the semi-discrete KT central scheme when a source term is present reads

$$\frac{\mathrm{d}}{\mathrm{d}t} w_j(t) = -\frac{H_{j+1/2}(t) - H_{j-1/2}(t)}{\Delta x} + G_j(t) \tag{39}$$

where, assuming for the forcing term z a linear behaviour in terms of x inside the integration intervals, we obtain,

$$\begin{aligned} G_j(t) &= \frac{1}{\Delta x}\left[\int_{x_{j-1/2,r}}^{x_{j+1/2,l}} z(w(x,t))\,\mathrm{d}x + \int_{x_{j+1/2,l}}^{x_{j+1/2,r}} z(w(x,t))\,\mathrm{d}x\right] \\ &\simeq \frac{1}{2\Delta x}[(z(w_{j-1/2,r}^{n+1/2}) + z(w_{j+1/2,l}^{n+1/2}))\Delta x_j + (z(w_{j+1/2,l}^{n+1/2}) + z(w_{j+1/2,r}^{n+1/2}))\Delta x_{j+1/2}] \end{aligned} \tag{40}$$

here, the midpoint values are obtained from the corresponding Taylor expansions

$$w_{j\pm1/2,r}^{n+1/2} = w_{j\pm1/2,r}^{n} - \frac{\Delta t}{2}[f_x(w_{j\pm1/2,r}^{n}) - z(w_{j\pm1/2,r}^{n})] \tag{41a}$$

$$w_{j\pm1/2,l}^{n+1/2} = w_{j\pm1/2,l}^{n} - \frac{\Delta t}{2}[f_x(w_{j\pm1/2,l}^{n}) - z(w_{j\pm1/2,l}^{n})] \tag{41b}$$

Now, by setting $\Delta t \to 0$, from (41) and (22b), we obtain

$$w_{j\pm1/2,r}^{n+1/2} = w_{j+1/2}^{+}(t), \quad w_{j\pm1/2,l}^{n+1/2} = w_{j+1/2}^{-}(t)$$

In this way, the discretization of the source term (40) becomes

$$G_j(t) = \frac{1}{2\Delta x}[(z(w_{j-1/2}^{+}(t)) + z(w_{j+1/2}^{-}(t)))\Delta x_j + (z(w_{j+1/2}^{-}(t)) + z(w_{j+1/2}^{+}(t)))\Delta x_{j+1/2}] \tag{42}$$

3.3.3. Time integration of KT scheme. The integration in time of the set of ODE of the homogeneous and non-homogeneous semi-discrete second-order KT central schemes (35), and (39) represented as

$$\frac{\mathrm{d}w}{\mathrm{d}t} = \ell(w) \tag{43}$$

was performed by means of the following third-order TVD Runge–Kutta method, proposed by Shu and Osher [14],

$$\begin{aligned} w_0 &= w^n \\ w_1 &= w_0 + \Delta t\, \ell(w_0) \\ w_2 &= \frac{3}{4} w_0 + \frac{1}{4} w_1 + \frac{1}{4} \Delta t\, \ell(w_1) \\ w_3 &= \frac{1}{3} w_0 + \frac{2}{3} w_2 + \frac{2}{3} \Delta t\, \ell(w_2) \\ w^{n+1} &= w_3 \end{aligned} \tag{44}$$

Here, w^n stands for the variable vector evaluated at the time $t = n\Delta t$.

In the following numerical tests we have indicated by KT3 the semi-discrete KT central scheme, which uses for integration in time the third-order Runge–Kutta method of Shu and Osher, by NT the second-order Nessyahu and Tadmor scheme, and by LF the first-order Lax and Friedrichs scheme.

4. NUMERICAL APPLICATIONS

Dam-break and hydraulic jump phenomena, in idealized and real cases, have been simulated by using the above outlined LF, NT, and KT3 numerical schemes. We used for all tests a Courant number, $Cr = \max|\lambda_i|\Delta t/\Delta x = 0.9$. The results of the numerical tests with $Cr = 0.5$ have not pointed out relevant differences between NT and KT3 schemes, whereas, LF scheme gave slight dissipative solutions. We have assumed $\theta = 1.4$ as the optimal value to be used in (16) for the evaluation of the numerical derivatives in the NT scheme. It must be noted that $\theta = 2$ corresponds to the least dissipative condition, whereas, $\theta = 1$ corresponds to the most dissipative condition, which allows to avoid oscillations in the numerical solutions.

4.1. Idealized dam-break problem

In these tests we compare the analytical solutions with the numerical results obtained by the LF, NT, and KT3 schemes for an idealized dam-break problem for a rectangular, horizontal, and frictionless channel of length $L = 1000$ m. At the middle length of this channel there is initially located a dam. We indicate the water depth upstream and downstream of this dam, respectively, by $h_u = h(x, 0)$ for $x \leqslant 500$ m, and $h_d = h(x, 0)$ for $x > 500$ m. In the first set of the tests we used $h_u = 10$ m and $h_d = 0.1$ m (depth ratio $h_u/h_d = 100$) and, for the second set, $h_d = 0$ (depth ratio $h_u/h_d = \infty$). For all the tests we assumed $u(x, 0) = 0$. For boundary conditions we assumed $u(0, t) = u(L, t) = 0$.

At time $t = 0$, the dam is supposed to fully collapse instantaneously. In Figures 4–6 the results (depth and velocity) of the numerical simulations with LF, NT and KT3 schemes, for $h_u/h_d = 100$ and grid points $N = 1000$ are compared with the analytical solution [15] at

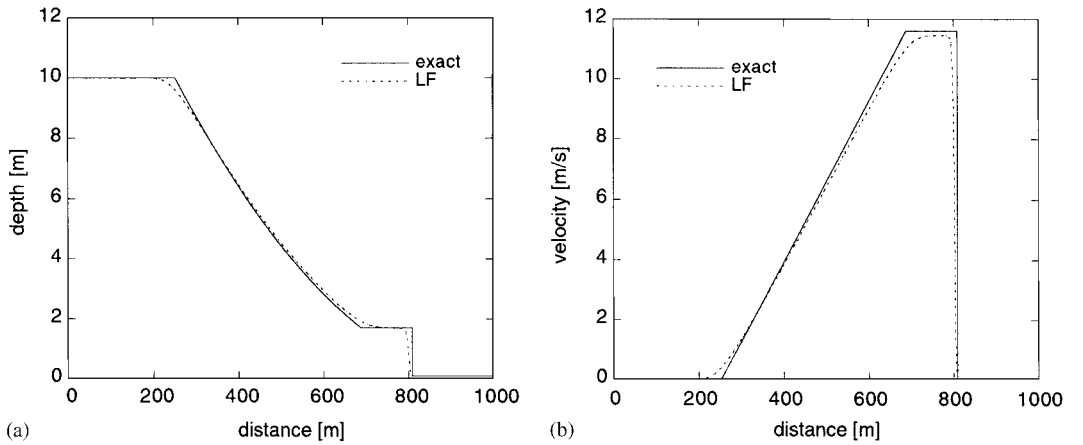

Figure 4. Depth ratio $h_u/h_d = 100$. Water profile (a) and velocity (b), for LF scheme, at $t = 25$ s.

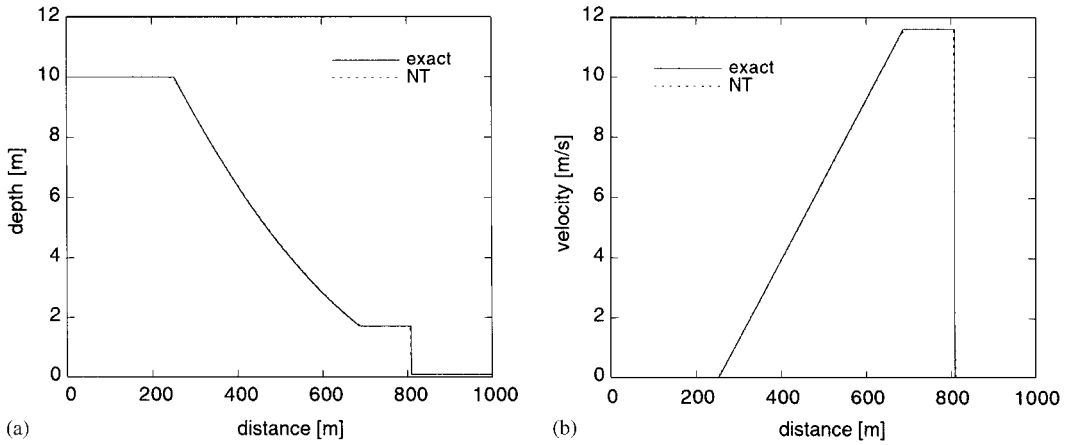

Figure 5. Depth ratio $h_u/h_d = 100$. Water profile (a) and velocity (b) for NT scheme, at $t = 25$ s.

$t = 25$ s. Analogously, the results of the simulations, for $h_u/h_d = \infty$ and $N = 1000$, at $t = 15$ s, are shown in Figures 7–9.

For evaluating the goodness of the approximation of the various schemes, the L_2-relative error

$$\delta_h = \left[\frac{\sum_i (h^n - h^e)^2}{\sum_i (h^e)^2}\right]^{\frac{1}{2}} \times 100 \tag{45}$$

was used. Here, h^n and h^e are the simulated and the exact depth, respectively. Analogous evaluation parameter δ_v was used for evaluating the goodness of the velocity. The numerical

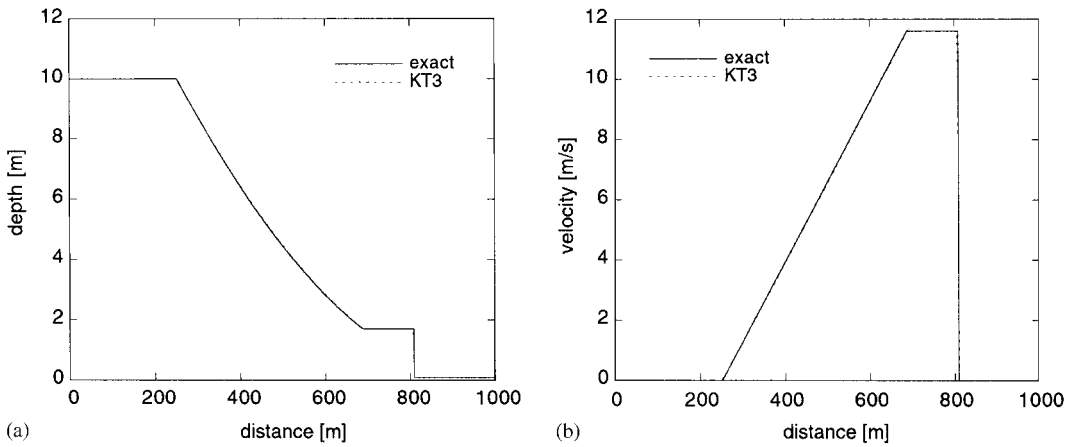

Figure 6. Depth ratio $h_u/h_d = 100$. Water profile (a) and velocity (b) for KT3 scheme, at $t = 25$ s.

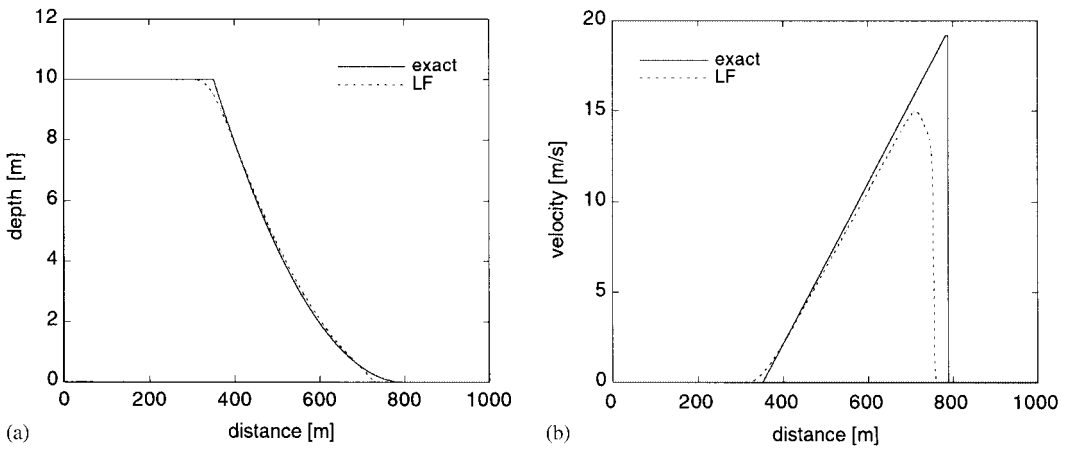

Figure 7. Depth ratio $h_u/h_d = \infty$. Water profile (a) and velocity (b) for LF scheme, at $t = 15$ s ($u_{max}^{ex} = 19.220$ m/s, $u_{max}^{LF} = 14.981$ m/s).

values obtained by the different models, in terms of the number of grid points N, used for the simulations, are summarized in Tables I and II.

From these tables we can see that the values of the δ_h and δ_v errors, as function of the number of grid points N, are very similar for the NT and KT3 schemes, whereas, those obtained by the LF scheme are greater than those obtained by the NT and KT3 schemes.

4.2. Dam-break experiment

In this test, we compare the laboratory dam-break experimental results of the Waterway Experiment Station (W.E.S.), U.S. Army Corps of Engineers [16], with the numerical simulations

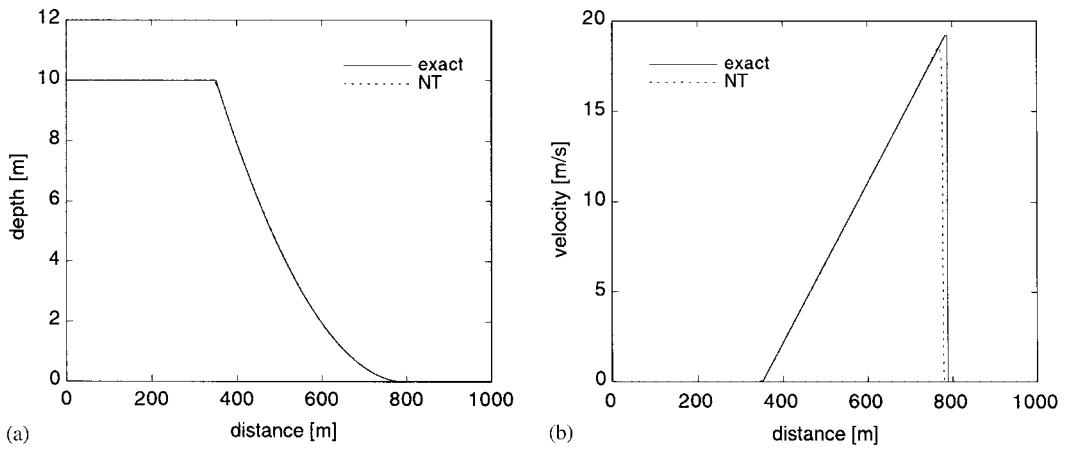

Figure 8. Depth ratio $h_u/h_d = \infty$. Water profile (a) and velocity (b) for NT scheme, at $t = 15$ s ($u_{max}^{ex} = 19.220$ m/s, $u_{max}^{NT} = 18.601$ m/s).

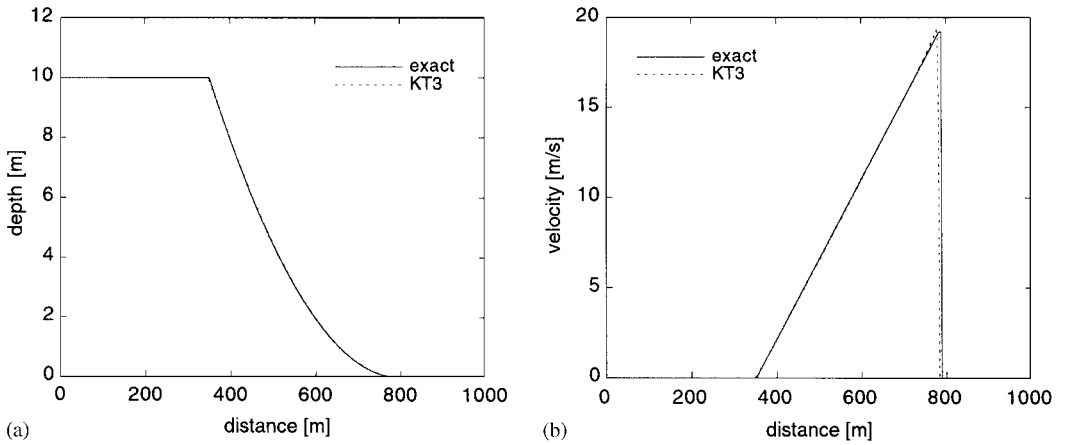

Figure 9. Depth ratio $h_u/h_d = \infty$. Water profile (a) and velocity (b) for KT3 scheme, at $t = 15$ s ($u_{max}^{ex} = 19.220$ m/s, $u_{max}^{KT3} = 19.349$ m/s).

obtained by LF, NT and KT3 schemes. The tests refer to a rectangular channel, 122m long and 1.22 m wide, with bottom slope $S_0 = 0.005$ and a Manning coefficient $n_m = 0.0085$ ($m^{-1/3}$ s). The water depth upstream of the dam, placed at the middle length, is 0.305 m and the downstream is zero. The grid size Δx is 0.5 m. Figures 10 show the measured and the simulated water profiles along the centreline of the flume at $t = 10$ (a), 20 (b), and 30 s (c), respectively. The hydrographs for the section at $x = 48.8$ (a), 61.0 (b), 68.5 (c), 70.1 (d) and 87.0 m (e),

Table I. Depth ratio $h_u/h_d = 100$: δ_h and δ_v, at $t = 25$ s, in term of N, for the various schemes.

N	LF	NT	KT3
δ_h			
250	4.402141	1.118037	9.7900E-1
500	3.441963	6.5036E-1	6.0018E-1
1000	2.589958	3.4073E-1	3.5410E-1
2000	2.016159	2.1675E-1	2.7500E-1
4000	1.582103	2.0940E-1	1.6879E-1
8000	1.210521	1.1429E-1	1.1474E-1
δ_v			
250	15.068930	5.400775	6.043134
500	15.684550	4.141970	4.219201
1000	13.727794	3.693018	3.358874
2000	12.121000	2.709816	3.443914
4000	10.293944	1.371508	1.595128
8000	8.223022	1.093976	1.589934

Table II. Depth ratio $h_u/h_d = \infty$: δ_h and δ_v, at $t = 15$ s, in term of N, for the various schemes.

N	LF	NT	KT3
δ_h			
250	3.400637	8.2128E-1	8.3571E-1
500	2.317644	4.1782E-1	4.2727E-1
1000	1.541604	2.0874E-1	2.1734E-1
2000	1.003548	1.0224E-1	1.1014E-1
4000	6.4198E-1	4.9248E-2	5.5776E-2
8000	4.0512E-1	2.3833E-2	2.8261E-2
δ_v			
250	45.252220	23.38548	20.57145
500	46.863830	27.32224	23.63476
1000	46.692930	25.69966	18.62127
2000	45.482330	21.72660	13.30657
4000	42.420654	16.38841	8.67526
8000	38.681823	11.32689	5.57758

respectively, are shown in Figures 11. These tests show good agreement between experimental and simulated results, also if the better comparison with the experimental data is obtained by the NT and KT3 schemes.

4.3. Hydraulic jump problem

In these tests the hydraulic jump is simulated. The results of these simulations, obtained by LF, NT, and KT3 schemes, are compared with the laboratory experiments on a rectangular

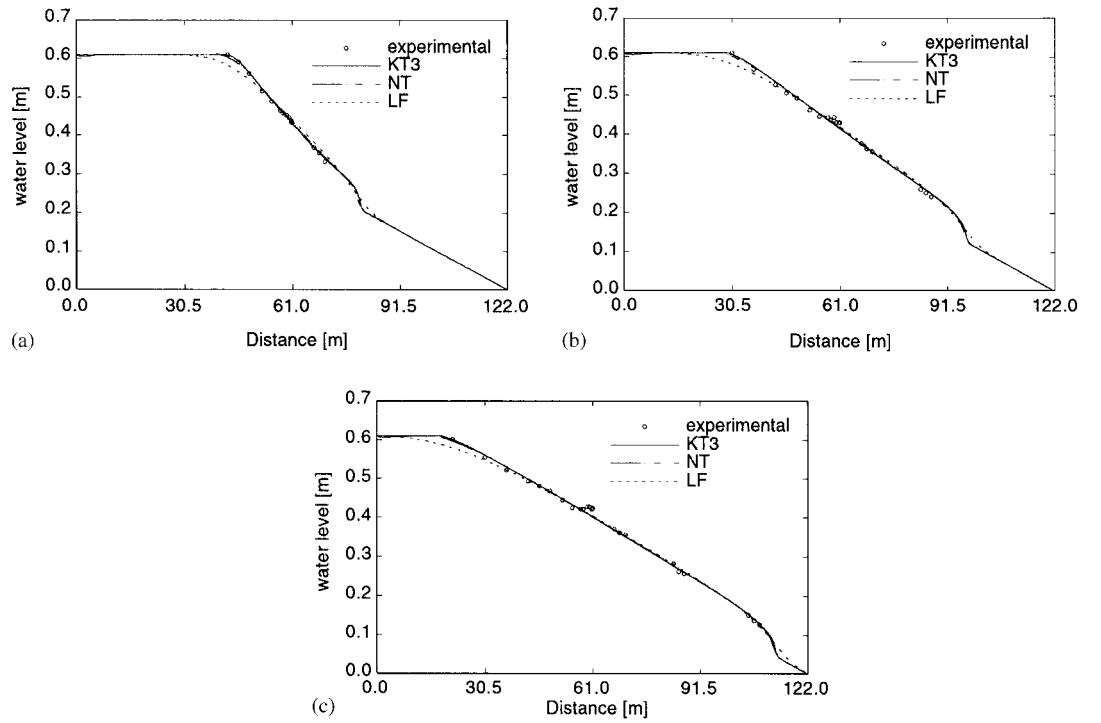

Figure 10. Water surface profiles at $t = 10$ (a), 20 (b) and 30 s (c).

channel, width $B = 0.46$m and length $L = 14$m, with bed slope $S_0 = 0$ and Manning's roughness coefficient $n_m = 0.008$ ($\mathrm{m}^{-1/3}$ s) [17]. The space interval $\Delta x = 0.1$ m was used.

In the first test, with a Froude number $Fr = 4.23$, the following initial and boundary conditions were used: $u(x,0) = 2.737$m/s, $h(x,0) = 0.043$m, and $h(0,t) = 0.043$m, $u(L,t) = 0.530$m/s. The steady-state water profiles for the three methods, reached at time of about $t = 150$ s, with $h(L,150) = 0.222$ m, are shown in Figure 12.

In the second test, with $Fr = 6.65$, we have used the following initial and boundary conditions: $u(0,x) = 3.255$ m/s, $h(x,0) = 0.024$ m, and $h(0,t) = 0.024$ m, $u(L,t) = 0.401$ m/s. The steady-state water profiles of these simulations, with $h(L,t) = 0.195$m, are shown in Figure 13. From the results shown in Figures 11 and 12, we can observe an acceptable similarity between experimental and simulated results.

5. CONCLUSIONS

The results obtained by using LF, NT and KT3 central schemes, to integrate the Saint-Venant equations for modelling dam-break and jump phenomena in open-channel flow, lead to the following conclusions:

1. The presented approximated extension of the NT and KT methods to the non-homogeneous case seems to have not reduced the accuracy obtained by these meth-

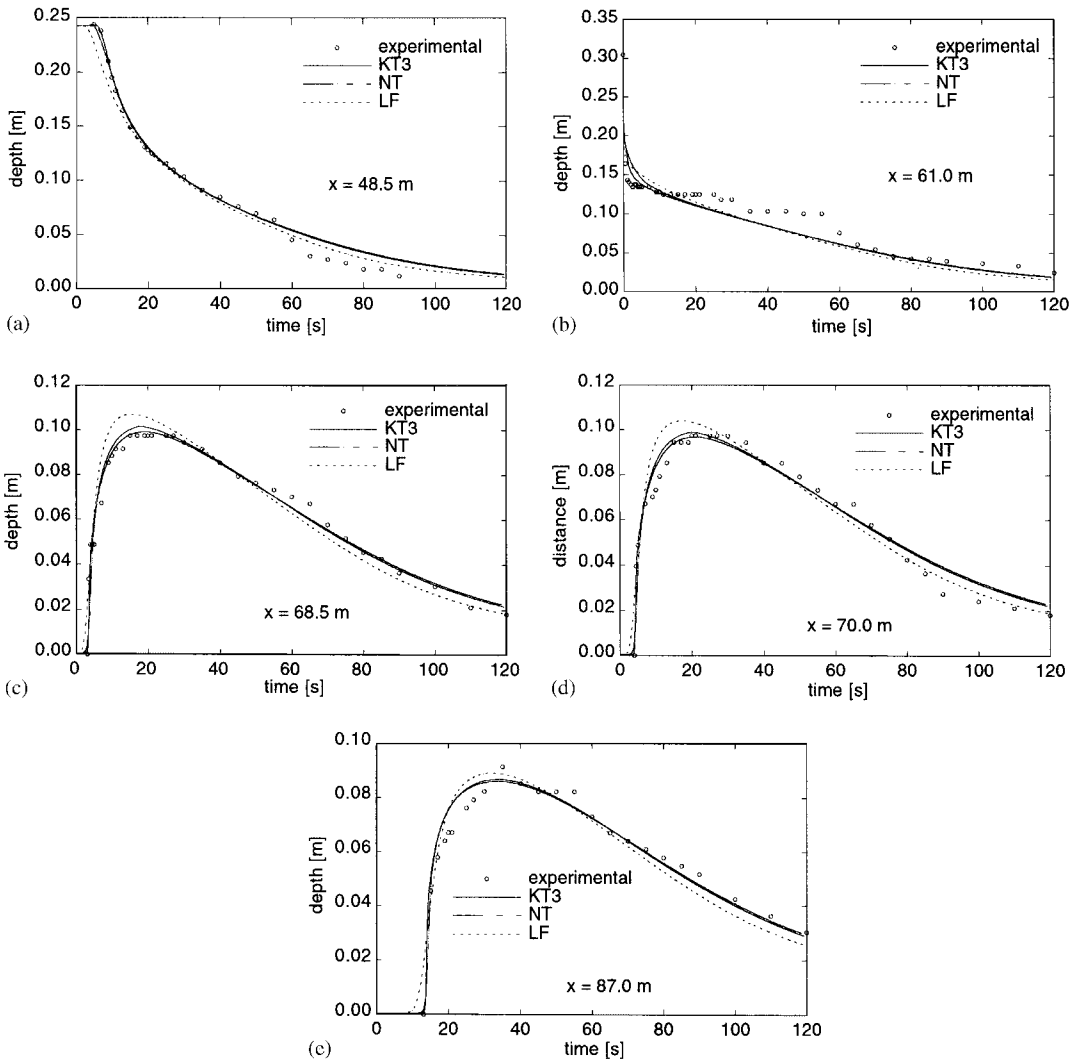

Figure 11. Hydrographs at points: $x = 48.8$ (a), 61.0 (b), 68.5 (c) 70.1 (d) and 87.0 m (e).

ods in the homogeneous cases. However it can be seen, by comparing the results of the idealized dam-break problem with the other test cases presented.

2. The NT and KT central schemes may be used for accurately modelling shock phenomena in open-channel flow governed by the non-linear set of homogeneous and non-homogeneous hyperbolic Saint-Venant equations.
3. The results obtained by the second-order NT scheme and the third-order in time KT3 scheme are comparable, whereas, as expected, the LF scheme gives slight dissipative solutions.

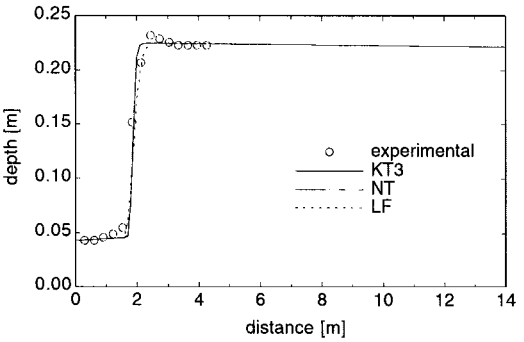

Figure 12. Hydraulic jump for $Fr = 4.23$.

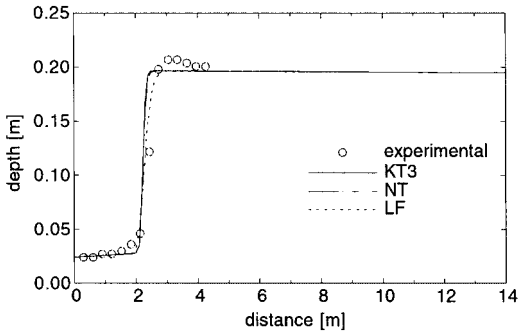

Figure 13. Hydraulic jump for $Fr = 6.65$.

4. Further experimentation of these methods in engineering problems may be necessary in solving two-dimensional overland flow and non-linear convention–diffusion transport problems.

REFERENCES

1. Hirsch C. *Numerical Computation of Internal and External Flows*, vol. 2. Wiley: Chichester, 1995.
2. Godunov SK. A difference scheme for numerical computation of discontinuous solution of hydrodynamic equations. *Mathematics Sbornik* 1959; **47**:271–306.
3. Friedrichs KO. Symmetric hyperbolic linear differential equations. *Communications on Pure and Applied Mathematics* 1954; **VII**:345–392.
4. Lax PD. Weak solutions of non-linear hyperbolic equations and their numerical computation. *Communications on Pure and Applied Mathematics* 1954; **VII**:159–193.
5. Nessyahu H, Tadmor E. Non-oscillatory central differencing for hyperbolic conservation laws. *Journal of Computational Physics* 1990; **87**:408–463.
6. Kurganov A, Tadmor E. New high-resolution central schemes for non-linear conservation laws and convection-diffusion equations. *Journal of Computational Physics* 2000; **160**:241–282.
7. Cunge JA, Holly JrFM, Verwey A. *Practical Aspects of Computational River Hydraulics*. Pitman: London, 1980.
8. Liu XD, Tadmor E. Third order nonoscillatory central scheme for hyperbolic conservation laws. *Numerische Mathematik* 1998; **79**:397–425.

9. Erbes G. A high-resolution Lax–Friedrichs scheme for hyperbolic conservation laws with source terms: application to the shallow water equations. Department of Meteorology Stockholm University, *Report DM-62*, March 1992.
10. Van Leer B. Towards the ultimate conservative difference scheme. V. A Second-Order Sequel to Godunov's Methods. *Journal of Computational Physics* 1979; **32**:101–136.
11. Jiang GS, Levy D, Lin CT, Osher S, Tadmor E. High-Resolution nonoscillatory central schemes with nonstaggered grids for hyperbolic conservation laws. *SIAM Journal of Numerical Analysis* 1998; **35**: 2147–2168.
12. Liotta SF, Romano V, Russo G. Central schemes for balance laws of relaxation type. *SIAM Journal of Numerical Analysis* 2000; **38**:1337–1356.
13. Kurganov A, Levy D. A third-order semidiscrete central scheme for conservation laws and convection-diffusion equations. *SIAM Journal on Scientific Computing* 2000; **22**:1461–1488.
14. Shu CW, Osher S. Efficient implementation of essentially non-oscillatory shock-capturing schemes. *Journal of Computational Physics* 1988; **77**:439–471.
15. Stoker JJ. *Water Waves*. Interscience Publishers: New York, 1957.
16. W.E.S. (Waterways Experiment Station) Floods resulting from suddenly breached dams, Misc. *Paper N. 2-374*, Report 1: Conditions of Minimum Resistance, 1960; Report 2: Conditions of High Resistance, 1961, U.S. Army Corps of Engineering, Vicksburg, Miss., U.S.A., 1960.
17. Gharangik AM, Chaudhry MH. Numerical simulation of hydraulic jump. *Journal of Hydraulic Engineering* 1991; **117**:1195–1211.

